.

# Initial Conditions
# for Direct Numerical Simulation
# of Turbulence

Stewart Cant

# 1 Introduction

In the Direct Numerical Simulation (DNS) of turbulent flow it is desirable to specify initial conditions that are already a good approximation to a turbulent solution of the Navier–Stokes equations. This ensures that the simulation will begin to generate a truly turbulent solution as quickly as possible and without excessive initial transients. It is also convenient to make use of the initial conditions to set the values of key turbulence parameters *a proiri*. In the absence of a Navier–Stokes solution in closed form, or of sufficiently–detailed experimental data, it is necessary to construct the initial approximation numerically. The output from a previous simulation may be used if the physical and computational parameters are compatible but it is more often the case that an entirely new set of turbulent initial conditions is required, for example where the computational domain size is to be changed or a new statistical realisation of the turbulence is needed. This report gives a detailed account of a method for producing an excellent numerical approximation to a field of three–dimensional homogeneous isotropic turbulence having a specified energy spectrum and satisfying the continuity constraint for incompressible flow. The method was suggested by Orszag [1] in the context of DNS using spectral methods and was refined by Rogallo [2] and by Lee and Reynolds [3]. Subsequently it has become a standard procedure for generating turbulent initial conditions for DNS, and this report describes its implementation in both serial and parallel codes for DNS of turbulent combustion.

It is worth noting that the restriction to incompressible flow allows for significant simplifications in both the mathematical formulation and the computational implementation of the turbulent initial velocity field. In practice this does not preclude the use of such an initial field to start a compressible or reacting flow simulation, provided that the subsequent evolution of the additional physics is well described.

Thus the aim is to generate a field of incompressible homogeneous isotropic turbulence having a specified energy spectrum function $E(\bar{k})$, where $\bar{k}$ is the wavenumber vector magnitude in the Fourier–space representation of the turbulent velocity field. Note that $\bar{k}$ is defined as a *linear* wavenumber or inverse wavelength, as distinct from an *angular* wavenumber with vector magnitude $\hat{k} = 2\pi\bar{k}$ which is used extensively in the classical literature. The function $E(\bar{k})$ is central to the procedure, since it defines among other things the initial value of the turbulence RMS fluctuation magnitude $u$, the turbulence integral length scale $L$, the Taylor length scale $\lambda$ and the Kolmogorov length scale $\eta$, as well as the turbulence energy dissipation rate $\varepsilon$.

The remainder of the report contains a brief account of the underlying theory as presented in detail by Batchelor [4], together with a discussion of the properties of the spectrum function and its relationship to the principal properties of the turbulence. This is followed by a description of the computational implementation of the method for generating turbulent initial conditions.

# 2 Theoretical Development

The intention is to ensure that the initial turbulent velocity field satisfies the conditions for continuity, homogeneity and isotropy. From the theoretical standpoint it is most convenient to do this in Fourier space.

## 2.1 Continuity

For incompressible flow the continuity condition is

$$\nabla.\underline{u} = 0 \tag{1}$$

which may be expressed in Fourier space as

$$\bar{k}.\hat{\underline{u}}(\underline{k}) = 0 \tag{2}$$

where $\hat{\underline{u}}(\bar{k})$ is the Fourier transform of the real–space velocity vector $\underline{u}(\underline{x})$:

$$\hat{\underline{u}}(\bar{k}) = \int \underline{u}(\underline{x}) \exp{(i2\pi\bar{k}.\underline{x})}d\underline{x} \tag{3}$$

$$\underline{u}(\underline{x}) \quad = \quad \int \hat{\underline{u}}(\underline{\bar{k}}) \exp\left(-i2\pi\underline{\bar{k}}.\underline{x}\right)d\underline{\bar{k}} \tag{4}$$

Note that the Fourier transform is defined here using standard modern practice, and that this differs in matters of detail from the older definition used by Batchelor [4]. In order for the integrals in (3) and (4) to exist it is necessary for the real–space velocity $\underline{u}$ to satisfy certain criteria [4], and in practice it is sufficient as well as simple and elegant to assume that $\underline{u}$ is periodic in all three directions.

## 2.2   Homogeneity

An important quantity to consider is the velocity correlation tensor $R_{ij}(\underline{r})$ defined as

$$R_{ij}(r) = \overline{u_i(\underline{x})u_j(\underline{x}+\underline{r})} \tag{5}$$

where the overbar indicates a time, space or ensemble average over the probability distribution of the velocity. The condition of homogeneity is assured by noting that $R_{ij}$ is a function of the spacing vector $\underline{r}$ only and does not depend on the position vector $\underline{x}$. As the spacing $\underline{r}$ tends to zero the velocity correlation tensor reduces to the Reynolds stress tensor

$$r_{ij} = R_{ij}(0) = \overline{u_i(\underline{x})u_j(\underline{x})} \tag{6}$$

which is independent of spatial position due to the assumption of homogeneity. The trace of the Reynolds stress tensor is equal to twice the turbulent kinetic energy per unit mass, ie

$$K = \frac{1}{2}r_{ii} = \frac{1}{2}\overline{u_i(\underline{x})u_i(\underline{x})} \tag{7}$$

The Fourier transform of $R_{ij}$ is the energy spectrum tensor $\Phi_{ij}$ defined as

$$\Phi_{ij}(\underline{\bar{k}}) = \int R_{ij}(\underline{r}) \exp\left(i2\pi\underline{\bar{k}}.\underline{r}\right)d\underline{r} \tag{8}$$

and the physical meaning of this tensor can be made clear by considering the inverse transform

$$R_{ij}(\underline{r}) = \int \Phi_{ij}(\underline{\bar{k}}) \exp\left(-i2\pi\underline{\bar{k}}.\underline{r}\right)d\underline{\bar{k}} \tag{9}$$

Setting the spacing vector $\underline{r}$ to zero in this expression yields

$$R_{ij}(0) = r_{ij} = \int \Phi_{ij}(\underline{\bar{k}})d\underline{\bar{k}} \tag{10}$$

so that $\Phi_{ij}$ is shown to describe the contribution to the correlation tensor $R_{ij}$ arising from each element of wavenumber in Fourier space. In particular, it follows that half of the trace $\Phi_{ii}$ of the energy spectrum tensor represents the energy density of the turbulence in Fourier space:

$$K = \frac{1}{2}r_{ii} = \int \frac{1}{2}\Phi_{ii}(\underline{\bar{k}})d\underline{\bar{k}} \tag{11}$$

A slightly different perspective is obtained by averaging $\Phi_{ij}$ over all directions in Fourier space according to

$$\Psi_{ij}(k) = \int \Phi_{ij}(\underline{\bar{k}})dA(\bar{k}) \tag{12}$$

where $\bar{k} = \sqrt{k_i k_i}$ is the wavenumber vector magnitude and $dA(\bar{k})$ denotes an element of the area of a sphere in Fourier space at radius $\bar{k}$. Then the directionally–averaged tensor $\Psi_{ij}(\bar{k})$ represents the contribution to the energy spectrum tensor from a small element of wavenumber magnitude $d\bar{k}$ forming a spherical shell at radius $\bar{k}$.

3

In passing, it is useful to note that the one–dimensional spectrum functions $\Theta_{ij}$ may be obtained by integrating the energy spectrum tensor over two of the components of the vector argument $\underline{\bar{k}}$. Choosing without loss of generality to take $\bar{k}_1$ as the surviving component yields

$$\Theta_{ij}(\bar{k}_1) = \int_{-\infty}^{\infty} \int_{-\infty}^{\infty} \Phi_{ij}(\bar{k}_1, \bar{k}_2, \bar{k}_3) dk_2 dk_3. \tag{13}$$

The longitudinal one–dimensional spectrum function $\Theta_{11}(\bar{k}_1)$ is obtained by setting $i = j = 1$, while the lateral one–dimensional spectrum functions $\Theta_{22}(\bar{k}_1)$ or $\Theta_{33}(\bar{k}_1)$ are obtained by setting $i = j \neq 1$.

## 2.3 Isotropy

The condition of isotropy is met by noting that the tensor $\Phi_{ij}$ must have a specific form in isotropic turbulence [4]:

$$\Phi_{ij}(\underline{\bar{k}}) = F_k(\bar{k}) \bar{k}_i \bar{k}_j + G_k(\bar{k}) \delta_{ij} \tag{14}$$

where $F_k$ and $G_k$ are functions only of the wavenumber vector magnitude. Using the continuity condition (2) it may be shown that

$$\frac{\partial}{\partial r_i} R_{ij} = \frac{\partial}{\partial r_j} R_{ij} = 0 \tag{15}$$

and from the definition (9) it follows that

$$\bar{k}_i \Phi_{ij} = \bar{k}_j \Phi_{ij} = 0. \tag{16}$$

Then the functions $F_k$ and $G_k$ are seen to be related according to $G_k = -\bar{k}^2 F_k$, and the tensor $\Phi_{ij}$ is specified completely by a single function $F_k$ of wavenumber vector magnitude. Since the turbulence is isotropic then by definition there is no preferred direction and the surfaces of constant energy in Fourier space are spheres. The energy contained within a spherical shell of thickness $d\bar{k}$ at a wavenumber magnitude $\bar{k}$ is defined as $E(\bar{k})d\bar{k}$ where $E(\bar{k})$ is the energy spectrum function. According to this definition together with (12) the energy spectrum function is given by

$$E(\bar{k}) = \frac{1}{2} \Psi_{ii}(\bar{k}) = \frac{1}{2} \Phi_{ii}(\bar{k}) \int dA(\bar{k}) \tag{17}$$

where the second step follows due to isotropy. Thus the energy spectrum function becomes

$$E(\bar{k}) = 4\pi \bar{k}^2 \frac{1}{2} \Phi_{ii}(\underline{\bar{k}}) \tag{18}$$

and the energy spectrum tensor for homogeneous isotropic turbulence is fully defined by

$$\Phi_{ij}(\underline{\bar{k}}) = \frac{E(\bar{k})}{4\pi \bar{k}^4} (\bar{k}^2 \delta_{ij} - \bar{k}_i \bar{k}_j) \tag{19}$$

In order to obtain expressions for the individual Fourier–space velocity components $\hat{u}_i(\bar{k})$ it is necessary to relate these to the spectrum tensor. Batchelor [4] notes that the physical–space velocity is given by

$$\underline{u}(\underline{x}) = \int \exp(-i2\pi \underline{\bar{k}}.\underline{x}) d\underline{Z}(\underline{\bar{k}}) \tag{20}$$

where $d\underline{Z}(\bar{k})$ is a vector of statistically independent random increments. Comparing with the Fourier transform definition (4) it is clear that in the present case $d\underline{Z}(\bar{k}) = \underline{\hat{u}}(\bar{k}) d\underline{\bar{k}}$, so that the Fourier–space velocity values $\underline{\hat{u}}(\bar{k})$ must themselves be random in nature. Substituting (20) in the definition (8) of the spectrum tensor it follows that

$$\Phi_{ij}(\underline{\bar{k}}) = \overline{\hat{u}_i(-\underline{\bar{k}}) \hat{u}_j(\underline{\bar{k}})} \tag{21}$$

and since the velocity in physical space is purely real the symmetry condition

$$\hat{u}_i(-\underline{\bar{k}}) = \hat{u}_j^*(\underline{\bar{k}}) \tag{22}$$

may be applied, where $*$ denotes the complex conjugate, so that

$$\Phi_{ij}(\underline{\bar{k}}) = \overline{\hat{u}_i^*(\underline{\bar{k}})\hat{u}_j(\underline{\bar{k}})} \tag{23}$$

Note that this result is different from that obtained using the correlation theorem in the case where the Fourier–space velocities are deterministic. In the present case it is necessary also to average over the probability space of the random velocity components. The implication is that the energy spectrum, as well as the conditions of homogeneity and isotropy, is accurate only in a statistical sense and that individual realisations of the velocity field may deviate significantly from the specified average.

# 3   Synthesis of the Initial Velocity Field

In constructing a realisation of the velocity field it is useful to note that the continuity equation (2) states that the Fourier–space velocity vector $\hat{\underline{u}}$ is orthogonal to the wavenumber vector $\underline{\bar{k}}$. Thus there is no component of $\hat{\underline{u}}$ in the direction of the wavenumber vector and it is possible to write an expression for the Fourier–space velocity vector having only two components:

$$\hat{\underline{u}}(\underline{\bar{k}}) = \alpha(\underline{\bar{k}})\underline{e}_1 + \beta(\underline{\bar{k}})\underline{e}_2 \tag{24}$$

Here, the system of unit basis vectors $\underline{e}_1$, $\underline{e}_2$ and $\underline{e}_3$ is defined such that $\underline{e}_3$ is aligned with $\underline{\bar{k}}$, and the complex functions $\alpha$ and $\beta$ are yet to be defined. In this coordinate system the trace of the spectrum tensor may be expressed using (23) and (24) as

$$\Phi_{ii}(\underline{\bar{k}}) = \frac{E(\bar{k})}{2\pi\bar{k}^2} = \overline{\alpha\alpha^* + \beta\beta^*} \tag{25}$$

In DNS it is possible to resolve only a limited range of scales, and a consequence is that the large scales of motion, while always well resolved, may be poorly sampled. In the present case the surfaces of constant energy in Fourier space are spheres, but the DNS computational grid corresponds in Fourier space to a regular cubic grid of points, each of which supports a single Fourier mode. The number of modes available to represent the motion up to a given energy level corresponds to the number of points contained within the sphere. For low wavenumbers the radius of the sphere is small and the number of modes is strictly limited. Physically this corresponds to the simple fact that only a small number of large eddies may be fitted into the computational box. Statistically the resulting small sample of large eddies may not be truly representative, and it is rarely possible to repeat the simulation many times in order to check the average expressed by the overbar in (23). A straightforward method which avoids this issue is to strengthen the condition implied by (25) and to insist that each Fourier mode must conform separately to the average energy:

$$\Phi_{ii}(\underline{\bar{k}}) = \frac{E(\bar{k})}{2\pi\bar{k}^2} = \alpha\alpha^* + \beta\beta^* \tag{26}$$

The simplest expressions for $\alpha$ and $\beta$ which satisfy this constraint are

$$\alpha = \sqrt{\frac{E(\bar{k})}{2\pi\bar{k}^2}} e^{i\theta_1} \cos\phi$$

$$\beta = \sqrt{\frac{E(\bar{k})}{2\pi\bar{k}^2}} e^{i\theta_2} \sin\phi \tag{27}$$

where $\theta_1$ and $\theta_2$ are phase angles defined on the interval $[-\pi, \pi)$, and $\phi$ is the azimuthal angle defined on the interval $[0, 2\pi)$ that specifies the angular position of the $\underline{e}_1$ vector in the plane normal to the

wavenumber vector $\bar{\underline{k}}$. In order to provide the degree of randomness required according to (20), all three angles are treated as uniformly–distributed random numbers with probability density functions

$$P_\theta(\theta_1) \;\; = \;\; \frac{1}{2\pi}, \;\; -\pi \le \theta_1 < \pi; \;\; 0 \text{ otherwise} \tag{28}$$

$$P_\theta(\theta_2) \;\; = \;\; \frac{1}{2\pi}, \;\; -\pi \le \theta_2 < \pi; \;\; 0 \text{ otherwise} \tag{29}$$

$$P_\phi(\phi) \;\; = \;\; \frac{1}{2\pi}, \;\; 0 \le \phi < 2\pi; \;\; 0 \text{ otherwise} \tag{30}$$

Having calculated the components of the Fourier–space velocity vector in the special coordinate system that has $\underline{e}_3$ aligned with $\underline{k}$ it is necessary to determine a rotation of axes that will provide the velocity components in the original coordinate system that defines the computational grid. The computational basis vectors are given by $\underline{b}_1 = (1, 0, 0)$, $\underline{b}_2 = (0, 1, 0)$, $\underline{b}_3 = (0, 0, 1)$, and in this coordinate system the $\underline{k}$-aligned basis vectors have components

$$
\begin{aligned}
\underline{e}_1 \;\; &= \;\; (e_{11}, e_{12}, e_{13}) \\
\underline{e}_2 \;\; &= \;\; (e_{21}, e_{22}, e_{23}) \\
\underline{e}_3 \;\; &= \;\; \left( \frac{\bar{k}_1}{\bar{k}}, \frac{\bar{k}_2}{\bar{k}}, \frac{\bar{k}_3}{\bar{k}} \right)
\end{aligned}
\tag{31}
$$

where the $e_{ij}$ are to be determined. Since the azimuthal angle $\phi$ is random there is freedom to choose the orientation of the $\underline{e}_1$ vector in the plane normal to $\underline{e}_3 = \bar{\underline{k}}$. It is convenient to fix $\underline{e}_1$ to lie within the $\underline{b}_1 - \underline{b}_2$ plane and this is achieved by setting $e_{13} = 0$. Then the remaining components follow from the orthogonality and normalisation conditions on the basis vectors to yield

$$
\begin{aligned}
\underline{e}_1 \;\; &= \;\; \left( \frac{\bar{k}_2}{M}, -\frac{\bar{k}_1}{M}, 0 \right) \\
\underline{e}_2 \;\; &= \;\; \left( \frac{\bar{k}_1 \bar{k}_3}{\bar{k} M}, \frac{\bar{k}_2 \bar{k}_3}{\bar{k} M}, -\frac{\bar{k}_1^2 + \bar{k}_2^2}{\bar{k} M} \right) \\
\underline{e}_3 \;\; &= \;\; \left( \frac{\bar{k}_1}{\bar{k}}, \frac{\bar{k}_2}{\bar{k}}, \frac{\bar{k}_3}{\bar{k}} \right)
\end{aligned}
\tag{32}
$$

where $M = \sqrt{\bar{k}_1^2 + \bar{k}_2^2}$. The rotation matrix required to transform a vector from the $\bar{\underline{k}}$-aligned basis into the computational basis is

$$
\underline{b}_{(i)} \cdot \underline{e}_{(j)} = \begin{pmatrix}
\frac{\bar{k}_2}{M} & \frac{\bar{k}_1 \bar{k}_3}{\bar{k} M} & \frac{\bar{k}_1}{\bar{k}} \\
-\frac{\bar{k}_1}{M} & \frac{\bar{k}_2 \bar{k}_3}{M} & \frac{\bar{k}_2}{\bar{k}} \\
0 & -\frac{\bar{k}_1^2 + \bar{k}_2^2}{M} & \frac{\bar{k}_3}{M}
\end{pmatrix}
\tag{33}
$$

and this may be applied to the Fourier–space velocity vector (24) to yield

$$
\begin{aligned}
\hat{u}_1(\bar{\underline{k}}) \;\; &= \;\; \frac{\alpha \bar{k} \bar{k}_2 + \beta \bar{k}_1 \bar{k}_3}{\bar{k} M} \\
\hat{u}_2(\bar{\underline{k}}) \;\; &= \;\; \frac{\beta \bar{k}_2 \bar{k}_3 - \alpha \bar{k} \bar{k}_1}{\bar{k} M} \\
\hat{u}_3(\bar{\underline{k}}) \;\; &= \;\; -\frac{\beta (\bar{k}_1^2 + \bar{k}_2^2)}{\bar{k} M}
\end{aligned}
\tag{34}
$$

## 3.1 Verification

It is simple to verify that the prescription given above exactly satisfies both the continuity condition (2) and the strengthened energy condition (26). Thus the single realisation of the turbulent velocity

field specified by (34) is divergence–free and conforms to the required energy spectrum function $E(\bar{k})$ in a deterministic manner. Substituting (34) in the expression (23) for the spectrum tensor $\Phi_{ij}(\underline{\bar{k}})$ it is possible to recover the expression (19) for the spectrum tensor in isotropic turbulence, but it is interesting to note that the condition for isotropy is satisfied only in the mean. For example, the component $\Phi_{11}$ is given by

$$
\begin{aligned}
\Phi_{11} &= \overline{\hat{u}_1^* \hat{u}_1} \\
&= \frac{1}{\bar{k}^2 M^2} \left[ \overline{\alpha^* \alpha} \bar{k}^2 \bar{k}_2^2 + (\overline{\alpha^* \beta} + \overline{\beta^* \alpha}) \bar{k} \bar{k}_1 \bar{k}_2 \bar{k}_3 + \overline{\beta^* \beta} \bar{k}_1^2 \bar{k}_3^2 \right]
\end{aligned} \tag{35}
$$

The averages denoted by the overbars on the terms in $\alpha$ and $\beta$ may be evaluated by substituting for $\alpha$ and $\beta$ from (27) and integrating over the probability density function for each of the angles $\theta_1$, $\theta_2$ and $\phi$:

$$
\begin{aligned}
\overline{\alpha^* \alpha} &= \frac{E(\bar{k})}{2\pi \bar{k}^2} \overline{\cos^2 \phi} = \frac{E(\bar{k})}{4\pi \bar{k}^2} \\
\overline{\alpha^* \beta} &= \frac{E(\bar{k})}{2\pi \bar{k}^2} \overline{e^{i(\theta_2 - \theta_1)} \cos\phi \sin\phi} = 0 \\
\overline{\beta^* \alpha} &= \frac{E(\bar{k})}{2\pi \bar{k}^2} \overline{e^{i(\theta_1 - \theta_2)} \cos\phi \sin\phi} = 0 \\
\overline{\beta^* \beta} &= \frac{E(\bar{k})}{2\pi \bar{k}^2} \overline{\sin^2 \phi} = \frac{E(\bar{k})}{4\pi \bar{k}^2}
\end{aligned} \tag{36}
$$

Thus the spectrum tensor component $\Phi_{11}$ becomes

$$
\Phi_{11} = \frac{E(\bar{k})}{4\pi \bar{k}^2} (\bar{k}^2 - \bar{k}_1^2)
$$

as required, and all of the remaining components follow in a similar manner. It is important to note that the averaging operation here is carried out notionally over an ensemble of many realisations of the turbulent velocity field, and that any single realisation may deviate significantly from isotropy due to the small sample of low–wavenumber modes.

It should also be noted that the prescription (34) does not automatically recover the symmetry condition expressed by (22), which must be imposed explicitly in order to ensure that the initial velocity field in physical space takes values that are purely real.

## 3.2  Limiting cases

In generating a velocity field using (34) some care is required when the denominator of each expression is equal to zero. This can occur when either $\bar{k} = 0$, or when $M = 0$ with $\bar{k}_3$ fixed and non–zero. When $\bar{k} = 0$ it is expected that the spectrum function $E(0)$ is identically zero. Given suitable limiting behaviour of $E(\bar{k})$ as $\bar{k} \to 0$, both $\alpha$ and $\beta$ are identically zero in the limit and no difficulty arises since all components $(\hat{u}_1, \hat{u}_2, \hat{u}_3)$ vanish. It is interesting to note that the manner in which $E(\bar{k}) \to 0$ as $\bar{k} \to 0$ has far–reaching theoretical consequences (see, for example, [7]).

By contrast, the case $M \to 0$, $\bar{k}_3 \neq 0$ in general has $E(\bar{k}) \neq 0$ and special consideration is required in the evaluation of the velocity components in order to produce the correct value of the turbulent kinetic energy. Since $\bar{k}^2 = M^2 + \bar{k}_3^2$, then as $M$ becomes much smaller than $\bar{k}_3$ it is clear that $\bar{k} \simeq \bar{k}_3$. Also, it is helpful to express $\bar{k}_1 = M \cos\psi$ and $\bar{k}_2 = M \sin\psi$ where $\psi$ is an angle in the $\bar{k}_1$–$\bar{k}_2$ plane. According to (34) the velocity components become

$$
\begin{aligned}
\hat{u}_1(\underline{\bar{k}}) &\simeq \frac{\alpha \bar{k}_2}{M} + \frac{\beta \bar{k}_1}{M} = \alpha \sin\psi + \beta \cos\psi \\
\hat{u}_2(\underline{\bar{k}}) &\simeq \frac{\beta \bar{k}_2}{M} - \frac{\alpha \bar{k}_1}{M} = \beta \sin\psi - \alpha \cos\psi \\
\hat{u}_3(\underline{\bar{k}}) &= 0
\end{aligned} \tag{37}
$$

The angle $\psi$ is arbitrary, since the azimuthal angle $\phi$ (see eq.27) has already been chosen at random and the energy condition (26) is satisfied automatically. Taking $\psi = \pi/2$ makes $\bar{k}_1 = 0$ and $\bar{k}_2 = M$, giving velocity components $\hat{u}_1 = \alpha$ and $\hat{u}_2 = \beta$. The randomness inherent in the definitions of $\alpha$ and $\beta$ remains unaffected, and the continuity and isotropy conditions are satisfied.

# 4 The Energy Spectrum Function

The energy spectrum function $E(\bar{k})$ plays a crucial role in defining the initial turbulence. It describes the distribution of turbulence kinetic energy in each spherical shell of Fourier space characterised by the linear wavenumber radius $\bar{k}$, such that the total kinetic energy per unit mass is given by

$$K = \frac{1}{2}\overline{u_i u_i} = \int_0^\infty E(\bar{k})d\bar{k} \tag{38}$$

The shape of the energy spectrum function has been measured experimentally in many different turbulent flows. In high–Reynolds–number flows which are a good approximation to incompressible homogeneous isotropic turbulence the spectrum has a characteristic form with identifiable portions corresponding to the energy–containing eddies, the inertial subrange and the dissipation range. The spectrum in the inertial subrange is governed by the well–known law $E(\bar{k}) \simeq \bar{k}^{-5/3}$, which may hold over a fairly broad range of wavenumber. In low Reynolds–number flows, or in flows where the turbulence has decayed, the inertial subrange becomes narrow and may disappear altogether leading to modified forms of the spectrum. Such modified forms are appropriate for the limited Reynolds numbers accessible in DNS.

The energy spectrum function also contains information about the turbulence energy dissipation rate, and about the length scales of the turbulence.

## 4.1 Turbulence Energy Dissipation Rate

In an incompressible homogeneous turbulent flow the energy dissipation rate per unit mass is given by (eg, [10])

$$\varepsilon = \nu\overline{\omega_i \omega_i} \tag{39}$$

where $\nu$ is the kinematic viscosity of the fluid and the vorticity vector is expressed as

$$\underline{\omega} = \nabla \times \underline{u} \text{ or } \omega_i = \epsilon_{ijk}\frac{\partial u_k}{\partial x_j} \tag{40}$$

where $\epsilon_{ijk}$ is the Levi–Civita symbol or permutation tensor. The link to the energy spectrum function is found by considering the vorticity correlation tensor $\overline{\omega_i(\underline{x})\omega_j(\underline{x}+\underline{r})}$. The Fourier transform of this tensor is the vorticity spectrum tensor

$$\Omega_{ij}(\underline{\bar{k}}) = \int \overline{\omega_i(\underline{x})\omega_j(\underline{x}+\underline{r})}\exp\left(i2\pi\underline{\bar{k}}.\underline{r}\right)d\underline{r} \tag{41}$$

with inverse transform

$$\overline{\omega_i(\underline{x})\omega_j(\underline{x}+\underline{r})} = \int \Omega_{ij}(\underline{\bar{k}})\exp\left(-i2\pi\underline{\bar{k}}.\underline{r}\right)d\underline{\bar{k}} \tag{42}$$

Setting the spacing vector $\underline{r} = 0$ and taking $i = j$ yields

$$\overline{\omega_i \omega_i} = \int \Omega_{ii}(\underline{\bar{k}})d\underline{\bar{k}} \tag{43}$$

from which it is clear that the vorticity spectrum tensor quantifies the contribution to the energy dissipation rate arising from each element of wavenumber space. This result may be compared with the analogous expression (11) for the turbulent kinetic energy.

Returning to the vorticity correlation tensor, and substituting for both $\omega_i(\underline{x})$ and $\omega_j(\underline{x}+\underline{r})$ from (40), it may be shown using the properties of the derivatives of the velocity correlation tensor [10] together with those of the permutation tensor [11] that

$$\overline{\omega_i(\underline{x})\omega_j(\underline{x}+\underline{r})} = -\delta_{ij}\frac{\partial^2}{\partial r_k \partial r_k}R_{ll}(\underline{r}) + \frac{\partial^2}{\partial r_i \partial r_j}R_{ll}(\underline{r}) + \frac{\partial^2}{\partial r_k \partial r_k}R_{ji}(\underline{r}) \tag{44}$$

Taking the Fourier transform of this expression yields the vorticity spectrum tensor in the form

$$\Omega_{ij}(\underline{\bar{k}}) = 4\pi^2 \left[\left(\bar{k}^2\delta_{ij} - \bar{k}_i\bar{k}_j\right)\Phi_{ll}(\underline{\bar{k}}) - \bar{k}^2\Phi_{ji}(\underline{\bar{k}})\right] \tag{45}$$

valid in homogeneous turbulence.

Restricting attention to isotropic turbulence, and using the form (19) for the energy spectrum tensor, the vorticity spectrum tensor for homogeneous isotropic turbulence becomes

$$\Omega_{ij}(\underline{\bar{k}}) = 4\pi^2 \left[\frac{E(\bar{k})}{4\pi\bar{k}^2}(\bar{k}^2\delta_{ij} - \bar{k}_i\bar{k}_j)\right] = 4\pi\bar{k}^2\Phi_{ij}(\bar{k})$$

Setting $i = j$ yields

$$\Omega_{ii}(\underline{\bar{k}}) = 4\pi^2\bar{k}^2\left[\frac{E(\bar{k})}{2\pi\bar{k}^2}\right]$$

and the dissipation rate follows by combining this expression with (39) and (43) to give

$$\varepsilon = 2\nu\int_0^\infty 4\pi^2\bar{k}^2 E(\bar{k})d\bar{k} \tag{46}$$

## 4.2   Integral Length Scales

The integral length scales in isotropic turbulence are determined by considering the longitudinal and lateral velocity correlation coefficients

$$\begin{aligned}
f(r) &= \frac{\overline{u_p(\underline{x})u_p(\underline{x}+\underline{r})}}{\overline{u_p^2}} \\
g(r) &= \frac{\overline{u_n(\underline{x})u_n(\underline{x}+\underline{r})}}{\overline{u_n^2}},
\end{aligned} \tag{47}$$

where $p$ and $n$ denote velocity components in directions respectively parallel and perpendicular to the spacing vector $\underline{r}$ whose magnitude is $r$, and there is no summation over subscripts $p$ and $n$. Then the longitudinal and lateral integral length scales are defined as

$$\begin{aligned}
L_p &= \int_0^\infty f(r)dr \\
L_n &= \int_0^\infty g(r)dr.
\end{aligned} \tag{48}$$

The correlation coefficients $f$ and $g$ may be expressed in terms of the velocity correlation tensor $R_{ij}(\underline{r})$ and hence in terms of the energy spectrum tensor $\Phi_{ij}(\underline{\bar{k}})$. In isotropic turbulence $R_{ij}(\underline{r})$ must have the form [4]

$$R_{ij}(\underline{r}) = F(r)r_i r_j + G(r)\delta_{ij} \tag{49}$$

where $F$ and $G$ are functions of the spacing vector magnitude $r$ only. Combining this form with the continuity condition on $R_{ij}$ (15) it follows that

$$4F + r\frac{\partial F}{\partial r} + \frac{1}{r}\frac{\partial G}{\partial r} = 0. \tag{50}$$

9

The correlation coefficients $f$ and $g$ are obtained in terms of $F$ and $G$ using (49) by setting $i = j$ respectively parallel and perpendicular to the direction of the vector $\underline{r}$:

$$
\begin{aligned}
u^2 f(r) &= \overline{u_p(\underline{x})u_p(\underline{x}+\underline{r})} = r^2 F(r) + G(r) \\
u^2 g(r) &= \overline{u_n(\underline{x})u_n(\underline{x}+\underline{r})} = G(r)
\end{aligned}
\tag{51}
$$

where

$$
u^2 = \overline{u_p^2} = \overline{u_n^2} = \frac{1}{3}\overline{u_i u_i} = \frac{2}{3}K
\tag{52}
$$

is the isotropic rms turbulent velocity fluctuation magnitude. Combining (49) with (51) yields

$$
R_{ij}(r) = u^2 \left\{ [f(r) - g(r)] \frac{r_i r_j}{r^2} + g(r)\delta_{ij} \right\}
\tag{53}
$$

while (50) produces a relation between $f$ and $g$:

$$
g = f + \frac{1}{2}rf',
\tag{54}
$$

Integration by parts is straightforward

$$
\int_0^\infty g\,dr = \int_0^\infty \left( f + \frac{1}{2}rf' \right) dr = \frac{1}{2}\int_0^\infty f\,dr
$$

and therefore from (48) the relation between the lateral and longitudinal integral length scales is shown to have the simple form

$$
L_n = \frac{1}{2}L_p.
$$

Using the definition of the spectrum tensor (8) and its form (19) in isotropic turbulence it is clear that

$$
\Phi_{ii}(\underline{\bar{k}}) = \frac{E(\bar{k})}{2\pi\bar{k}^2} = \int R_{ii}(\underline{r}) \exp\left( i2\pi\underline{\bar{k}}.\underline{r} \right) d\underline{r}.
$$

and from (53)

$$
R_{ii} = u^2 (f + 2g) = u^2 (3f + rf').
\tag{55}
$$

By analogy with the definition of the energy spectrum function (18) it is helpful to define the scalar function $R(r)$ as

$$
R(r) = \frac{1}{2}R_{ii}
\tag{56}
$$

whereupon $E(k)$ and $R(r)$ are seen to be related according to the Fourier transform

$$
\frac{E(\bar{k})}{4\pi\bar{k}^2} = \int R(r) \exp\left( i2\pi\underline{\bar{k}}.\underline{r} \right) d\underline{r}.
$$

Expressing both $\underline{r}$ and $\underline{\bar{k}}$ in spherical coordinates and integrating over all angles yields the one–dimensional Fourier transform pair

$$
\begin{aligned}
E(\bar{k}) &= 4 \int_0^\infty R(r)\bar{k}r \sin\left( 2\pi\bar{k}r \right) dr \\
R(r) &= \int_0^\infty E(\bar{k}) \frac{\sin\left( 2\pi\bar{k}r \right)}{2\pi\bar{k}r} d\bar{k}.
\end{aligned}
\tag{57}
$$

In order to obtain an expression for the longitudinal integral length scale $L_p$ in terms of $E(\bar{k})$ it is necessary to evaluate the integral of $R(r)$ as defined by (55) and (56):

$$
\int_0^\infty R(r)\,dr = \int_0^\infty \frac{u^2}{2}(3f + rf')\,dr = u^2 \int_0^\infty f(r)\,dr.
$$

10

Thus the integrals of $R(r)$ and $f(r)$ are seen to be closely related, and $L_p$ is found from its definition (48) together with (57):

$$L_p = \int_0^\infty f(r)dr = \frac{1}{u^2}\int_0^\infty R(r)dr = \frac{1}{u^2}\int_0^\infty\int_0^\infty E(\bar{k})\frac{\sin{(2\pi\bar{k}r)}}{2\pi\bar{k}r}d\bar{k}dr$$

to give the result

$$L_p = \frac{1}{u^2}\int_0^\infty \frac{E(\bar{k})}{4\bar{k}}d\bar{k}; \quad L_n = \frac{1}{2}L_p \tag{58}$$

or alternatively

$$L_p = \frac{3}{8}\frac{\int_0^\infty \frac{E(\bar{k})}{4\bar{k}}d\bar{k}}{\int_0^\infty E(\bar{k})d\bar{k}}; \quad L_n = \frac{1}{2}L_p. \tag{59}$$

## 4.3   Taylor Length Scale

The Taylor length scale $\lambda$ is found by considering the curvature of the velocity correlation coefficients $f(r)$ and $g(r)$ as the spacing vector magnitude $r$ tends to zero. From the definitions (47) it is clear that $f(0) = g(0) = 1$, and according to the Schwartz inequality [4] this must be the maximum value of both of these functions. Thus also $f'(0) = g'(0) = 0$, and a Taylor series expansion of $f(r)$ about the origin yields

$$f(r) = 1 + \frac{1}{2}f''(0)r^2 + O(r^4)$$

with $g(r)$ given in terms of $f(r)$ by (54). The definition of the Taylor length scale $\lambda$ is

$$f''(0) = -\frac{1}{\lambda}$$

so that for small values of $r$:

$$f(r) \simeq 1 - \frac{r^2}{2\lambda}$$
$$g(r) \simeq 1 - \frac{r^2}{\lambda}. \tag{60}$$

Now the expression (44) for the vorticity correlation tensor may be simplified for $i = j$ and $r = 0$ as

$$\overline{\omega_i\omega_i} = -\left(\nabla^2 R_{ii}\right)_{r=0}.$$

while the trace $R_{ii}$ of the velocity correlation tensor is given in terms of $f$ and $g$ by (55). Substituting for $R_{ii}$, differentiating twice and collecting terms of lowest order results in

$$\overline{\omega_i\omega_i} \simeq 15\frac{u^2}{\lambda^2}$$

Using (39) $\lambda$ may be expressed in terms of the energy dissipation rate as

$$\lambda^2 = \frac{15\nu u^2}{\varepsilon}$$

or using (38), (46) and (52), the result for $\lambda$ in terms of the energy spectrum function is

$$\lambda^2 = \frac{5\int_0^\infty E(\bar{k})d\bar{k}}{\int_0^\infty 4\pi^2\bar{k}^2 E(\bar{k})d\bar{k}} \tag{61}$$

11

## 4.4 Kolmogorov Length Scale

The Kolmogorov length scale is defined as

$$\eta = \left( \frac{\nu^3}{\varepsilon} \right)^{1/4}$$

and using (46) the result for $\eta$ in terms of $E(\bar{k})$ becomes

$$\eta = \left[ \frac{\nu^2}{2 \int_0^\infty 4\pi^2 \bar{k}^2 E(\bar{k}) d\bar{k}} \right]^{1/4} \tag{62}$$

It should be noted that there is no guarantee that the Kolmogorov length scale computed from the initial spectrum using (62) will be resolvable on the computational grid specified for the ensuing DNS. This is a basic compatibility requirement and must be checked separately.

# 5 Examples of Energy Spectrum Functions

Among the many forms that have been proposed for the energy spectrum function, only a few have found widespread use in the somewhat limited range of Reynolds number attainable in DNS. Some examples are given below.

## 5.1 Batchelor–Townsend Spectrum

This spectrum is widely used in DNS and is believed to be representative of the later stages of the decay of grid turbulence [6]. The spectrum is expressed as

$$E(k) = c_0 \frac{\bar{k}^4}{\bar{k}_0^5} e^{-2\left( \bar{k}/\bar{k}_0 \right)^2} \tag{63}$$

The form $\bar{k}^4$ for low wavenumbers corresponds strictly to the incompressible limit [4] while the Gaussian tail provides a rapid roll–off of the energy at high wavenumber. The parameters are the multiplier $c_0$ and the wavenumber $\bar{k}_0$ corresponding to the peak energy. Results for the quantities of interest are:

Turbulent kinetic energy

$$K = \frac{3}{32} \sqrt{\frac{\pi}{2}} c_0$$

Turbulence energy dissipation rate

$$\varepsilon = \frac{15}{16} \sqrt{\frac{\pi}{2}} \pi^2 \nu c_0 \bar{k}_0^2$$

Longitudinal integral length scale

$$L_p = \frac{1}{\sqrt{2\pi} \bar{k}_0}$$

Taylor length scale

$$\lambda^2 = \frac{1}{2\pi^2 \bar{k}_0^2}$$

Kolmogorov length scale

$$\eta = \left[ \frac{\nu^2}{\frac{15}{16} \sqrt{\frac{\pi}{2}} \pi^2 c_0 \bar{k}_0^2} \right]^{1/4}$$

## 5.2 Schumann–Patterson Spectrum

This spectrum was used by Schumann and Patterson [5] for simulations of turbulence in which the energy is concentrated at very low wavenumber. The form of the spectrum is particularly simple:

$$E(k) = c_0 \frac{\bar{k}}{\bar{k}_0^2} e^{-\bar{k}/\bar{k}_0} \tag{64}$$

The parameters are the multiplier $c_0$ and the wavenumber $k_0$ corresponding to the peak energy. Results for quantities of interest are:

Turbulent kinetic energy

$$K = \frac{3}{2} u^2 = c_0$$

Turbulent kinetic energy dissipation rate

$$\varepsilon = 48\pi^2 \nu c_0 k_0^2$$

Longitudinal integral length scale

$$L_p = \frac{3}{8k_0}$$

Taylor length scale

$$\lambda^2 = \frac{5}{24\pi^2 k_0}$$

Kolmogorov length scale

$$\eta = \left[ \frac{\nu^2}{48\pi^2 c_0 k_0} \right]^{1/4}$$

## 5.3 Lee–Reynolds Spectrum

This spectrum was used for simulations of homogeneous turbulence [3] and has the form

$$
\begin{aligned}
E(\bar{k}) &= \gamma_E \bar{k}^2; \quad \bar{k}_{\min} \leq \bar{k} \leq \bar{k}_p \\
E(\bar{k}) &= \gamma_E \bar{k}_p^2 \left( \frac{\bar{k}}{\bar{k}_p} \right)^{-5/3}; \quad \bar{k}_p < \bar{k} \leq \bar{k}_{\max} \\
E(\bar{k}) &= 0; \quad \text{otherwise}
\end{aligned} \tag{65}
$$

It combines a $\bar{k}^2$ dependence for low wavenumbers with a model inertial subrange having a $\bar{k}^{-5/3}$ dependence. The parameters are the multiplier $\gamma_E$, the wavenumber $\bar{k}_p$ corresponding to the peak energy, and the minimum and maximum wavenumbers $\bar{k}_{\min}$ and $\bar{k}_{\max}$ for which the spectrum is non–zero. Analytical integration of the spectrum according to (38), (46) and (59) produces the following results:

Turbulent kinetic energy

$$K = \frac{3}{2} u^2 = \frac{11}{6} \gamma_E \bar{k}_p^3 \left[ 1 - \frac{2}{11} \left( \frac{\bar{k}_{\min}}{\bar{k}_p} \right)^3 - \frac{9}{11} \left( \frac{\bar{k}_p}{\bar{k}_{\max}} \right)^{2/3} \right]$$

Turbulent kinetic energy dissipation rate

$$\varepsilon = 8\pi^2 \nu \frac{11}{20} \gamma_E \bar{k}_p^5 \left[ \frac{15}{11} \left( \frac{\bar{k}_p}{\bar{k}_{\max}} \right)^{-4/3} - \frac{4}{11} \left( \frac{\bar{k}_{\min}}{\bar{k}_p} \right)^5 - 1 \right]$$

Longitudinal integral length scale

$$L_p = \frac{9}{40} \frac{1}{\bar{k}_p} \frac{\left[ 1 - \frac{5}{11} \left( \frac{\bar{k}_{\min}}{k_p} \right)^2 - \frac{6}{11} \left( \frac{\bar{k}_p}{\bar{k}_{\max}} \right)^{5/3} \right]}{\left[ 1 - \frac{2}{11} \left( \frac{\bar{k}_{\min}}{k_p} \right)^3 - \frac{9}{11} \left( \frac{\bar{k}_p}{\bar{k}_{\max}} \right)^{2/3} \right]}$$

Taylor length scale

$$\lambda^2 = \frac{25}{6\pi^2} \frac{1}{\bar{k}_p^2} \frac{\left[ 1 - \frac{2}{11} \left( \frac{\bar{k}_{\min}}{k_p} \right)^3 - \frac{9}{11} \left( \frac{\bar{k}_p}{\bar{k}_{\max}} \right)^{2/3} \right]}{\left[ \frac{15}{11} \left( \frac{\bar{k}_{\max}}{k_p} \right)^{4/3} - \frac{4}{11} \left( \frac{\bar{k}_{\min}}{k_p} \right)^5 - 1 \right]}$$

Kolmogorov length scale

$$\eta = \left[ \frac{20}{88\pi^2 \gamma_E \bar{k}_p^5} \frac{\nu^2}{\left[ \frac{15}{11} \left( \frac{\bar{k}_p}{\bar{k}_{\max}} \right)^{-4/3} - \frac{4}{11} \left( \frac{\bar{k}_{\min}}{k_p} \right)^5 - 1 \right]} \right]^{1/4}$$

# 6  A Note on Wavenumber and Fourier Transform Definitions

All of the foregoing analysis has been conducted using the linear wavenumber $\bar{k}$ in place of the angular wavenumber $\hat{k} = 2\pi\bar{k}$ that is more common in the classical literature. This has been done mainly for computational reasons: the standard DNS domain is a unit cube whereupon the linear wavenumber is an integer and corresponds naturally to the indexing required for the FFT algorithm. It is a simple matter in each case to replace $\bar{k}$ with $\hat{k}/2\pi$ and to recover the classical result. Some caution is required in the case of the energy spectrum function: it is necessary to also replace $E(\bar{k})$ with $2\pi\hat{E}(\hat{k})$ where $\hat{E}(\bar{k})$ is the classical energy spectrum function.

Intermediate results may be affected by the present definition of the Fourier transform (3,4) which again reflects modern computational practice. For completeness, the older definition used by Batchelor [4] is

$$\hat{\underline{u}}(\bar{k}) = \frac{1}{8\pi} \int \underline{u}(\underline{x}) \exp\left(-i\hat{\underline{k}}.\underline{x}\right) d\underline{x}$$

$$\underline{u}(\underline{x}) = \int \hat{\underline{u}}(\hat{\underline{k}}) \exp\left(i\hat{\underline{k}}.\underline{x}\right) d\hat{\underline{k}} \tag{66}$$

# 7  Implementation

The Fourier–space velocity formulae (34) are to be used as the basis of a method for generating a turbulent initial velocity field for DNS in physical space. This requires (a) the evaluation of the Fourier space velocity values; (b) the imposition of symmetry condition (22); and (c) an inverse Fourier transform (4). A number of computational issues must be considered at the outset. It is envisaged that the DNS will be carried out on distributed memory parallel computers and the initial turbulence–generation algorithm must be designed to operate in the same environment. In computing terms the size of the DNS is necessarily large and so is the size of the required initial field. For reasons of computational efficiency it is essential to make use of the Fast Fourier Transform (FFT) in the inverse transform phase and this affects the design of the algorithm and the structure and indexing of the data.

The computational domain is a cuboid of size $(L_x, L_y, L_z)$ in physical space which is discretised on a set of evenly–spaced nodes numbered $(1 \ldots N_x, 1 \ldots N_y, 1 \ldots N_z)$, starting in the bottom–left–nearest corner. The numbers of nodes $N_x$, $N_y$ and $N_z$ in each direction need not be equal, and each may be even

or odd. The Fourier–space equivalent is a cuboid in (linear) wavenumber space of size $(N_x/L_x, N_y/L_y, N_z/L_z)$, with evenly–spaced nodes indexed as $(-N_x/2 \ldots N_x/2, -N_y/2 \ldots N_y/2, -N_z/2 \ldots N_z/2)$ where truncation of half–integer values is implied for odd $N_x$, $N_y$ or $N_z$, and the wavenumber origin is taken at (0,0,0) in the centre of the domain. Note that for even values of $N_x$, $N_y$ or $N_z$ each Fourier space grid line contains an extra node compared to the computational grid in physical space, but that the values of the Fourier coefficients at the end nodes $\pm N/2$ are necessarily equal and so no additional information is stored. Note also that for maximum benefit in using the FFT algorithm it is necessary for each of $(N_x, N_y, N_z)$ to be a product of powers of small prime factors [8].

The prescription (34) requires the energy spectrum function $E(\bar{k})$ to be specified *a priori*. It is clear from the analysis given above that it is possible to control the total kinetic energy, dissipation rate and principal length scales of the turbulence by making adjustments to the form and magnitude of the spectrum function alone. This is best done either analytically or numerically as a preprocessing exercise. A random number generator producing uniformly–distributed random deviates is also required in order to compute the random angles $\phi$, $\theta_2$ and $\theta_2$, and this is discussed in the Appendix.

The symmetry condition (22) requires the real (imaginary) part of each Fourier–space velocity component to be symmetric (antisymetric) about the origin in wavenumber space. This implies that velocity component values need to be specified at only half of the total number of nodes in the Fourier space, with the rest following by symmetry. This is consistent with specifying the velocity component values at every node in physical space, since each complex Fourier–space value contains twice as much information as a real value in physical space. There are several ways to implement the symmetry condition since the random nature of the Fourier coefficients allows a high degree of flexibility. A simple method is to initialise over the full domain and to impose symmetry by means of sums and differences at centrally–symmetric nodes [1]. Alternatively, random values may be computed over half the domain and each value stored appropriately at two centrally–symmetric locations. These approaches require immediate access to the entire computational domain in Fourier space and hence are difficult to implement efficiently on distributed–memory computers. The method adopted here is intended to overcome this limitation by exploiting the fact that a multidimensional Fourier transform can be viewed as a sequence of one–dimensional transforms. The three–dimensional inverse transform relation may be expressed as

$$u_i(x_1, x_2, x_3) = \int \int \int \hat{u}_i(\bar{k}_1, \bar{k}_2, \bar{k}_3) e^{-i2\pi \bar{k}_1 x_1} e^{-i2\pi \bar{k}_2 x_2} e^{-i2\pi \bar{k}_3 x_3} d\bar{k}_1 d\bar{k}_2 d\bar{k}_3 \qquad (67)$$

where the complex velocity component $\hat{u}_i$ must satisfy the symmetry condition (22) expressed as

$$\hat{u}_i(-\bar{k}_1, -\bar{k}_2, -\bar{k}_3) = \hat{u}_i^*(\bar{k}_1, \bar{k}_2, \bar{k}_3) \qquad (68)$$

When the Fourier transforms in the $x_1$ and $x_2$ directions are complete the three–dimensional transform becomes

$$u_i(x_1, x_2, x_3) = \int \hat{u}_i^{(1,2)}(x_1, x_2, \bar{k}_3) e^{-i2\pi \bar{k}_3 x_3} d\bar{k}_3 \qquad (69)$$

where $\hat{u}_i^{(1,2)}$ represents the partially–transformed velocity component. The important point is that $\hat{u}_i^{(1,2)}$ remains complex, whereas $u_i$ is real. Thus the three–dimensional central symmetry condition (22) must reduce to symmetry of the partial transform in the single direction $x_3$

$$\hat{u}_i^{(1,2)}(x_1, x_2, -\bar{k}_3) = \hat{u}_i^{*(1,2)}(x_1, x_2, \bar{k}_3) \qquad (70)$$

and this can be verified by expanding the transform relation (67) using De Moivre's theorem and collecting odd and even terms. Note that the choice of $x_3$ as a special direction is purely arbitrary, and that the foregoing argument is equally valid in any of the three coordinate directions.

The ability to impose symmetry in one direction, rather than centrally over the whole domain, allows for the entire initialisation procedure to be carried out in a very convenient manner. By symmetry, only half of the Fourier–space velocity values have to be computed. In the present case, $x_3$ is retained as the special direction and the upper half of the wavenumber domain $0 \leq \bar{k}_3 \leq N_z/2$ is filled with computed

data using the velocity formulae (34). An inverse Fourier transform is then carried out on all $\bar{k}_1$-$\bar{k}_2$ planes in this range in order to produce the partial transform defined by (69). The symmetry condition (70) is applied along each $x_3$-line, thus populating the lower half of the domain $-N_z/2 \leq \bar{k}_3 < 0$, and a further inverse Fourier transform in the $x_3$ direction completes the initialisation procedure.

Special treatment is required in the plane $\bar{k}_3 = 0$ which is not symmetric to any other. Here the upper half of the plane $\bar{k}_2 > 0$ is filled with computed velocity components and an inverse Fourier transform is applied along each line in the $\bar{k}_1$ direction. Symmetry is then imposed along $\bar{k}_1$-lines according to

$$\hat{u}_i^{(1)}(x_1, -\bar{k}_2, 0) = \hat{u}_i^{*(1)}(x_1, \bar{k}_2, 0)$$

followed by a further inverse Fourier transform in the $\bar{k}_2$ direction. Similarly the line $\bar{k}_2 = 0$ in the plane $\bar{k}_3 = 0$ requires special treatment since it is symmetric to no other. Here the velocity values for $\bar{k}_1 > 0$ are computed and symmetry is imposed along this single $\bar{k}_1$ line according to

$$\hat{u}_i(-\bar{k}_1, 0, 0) = \hat{u}_i^*(\bar{k}_1, 0, 0)$$

before inverse Fourier transformation in the same direction.

On a shared–memory computer the inverse FFT on each $\bar{k}_3$-plane may be carried out as a two–dimensional operation. Two–dimensional FFT routines do exist for distributed–memory architectures [9]. Nevertheless the most efficient of these require all data for the transform to be collected into the block of memory associated with a single processor, and after transformation the results must be returned to the correct remote location. Thus there is a significant overhead arising from the need to transfer data between processors, and a definite ceiling on the size of FFT that can be handled in the most efficient manner. Hence the present approach, developed in the context of a simple DNS domain–decomposition strategy, is to rely only on one–dimensional FFT routines. This makes it unlikely that the maximum possible FFT size will be reached in practical calculations and also simplifies the housekeeping associated with data transfer between processors.

# Appendix: Random Number Generators

The present method for initial turbulence generation requires three random numbers to be provided at each point in Fourier space. These are used in order to specify the phase angles $\theta_1$ and $\theta_2$ defined on the interval $[-\pi, \pi)$, and the azimuthal angle $\phi$ defined on the interval $[0, 2\pi)$, in each case with a uniform distribution across the interval. A reliable random number generator is required and for the purposes of DNS on a large domain it must be able to produce very large numbers of statistically independent random values. For example, DNS on a domain of $512^3$ points requires 402653184 independent random values for initialisation, while a domain of $1024^3$ points requires over 3 billion values. It is desirable to ensure that the properties of the random number generator are well understood and that the generator routine is portable between different computers and different compilers. A full account of the theory, implementation and testing of random number generators is given by Knuth [12].

## Linear Congruential Sequences

The simplest, fastest and most commonly–used method for generating a sequence of pseudo–random numbers is the linear congruential method. The recurrence relation

$$X_{n+1} = (aX_n + c)\,\mathrm{mod}\,m \tag{71}$$

is applied for $n \geq 0$, where $a$ is called the multiplier, $c$ the increment, $m$ the modulus and $X_0$ the starting value or seed. All of $a$,$c$,$m$ and $X_0$ are non–negative integers, with $m > a$, $m > c$ and $m > X_0$. Obviously the sequence of integer elements $X_n$ cannot be truly random since each element is computed deterministically, and indeed the $(n + k)$-th element for any $n, k \geq 0$ is given by the expression

$$X_{n+k} = \left( a^k X_n + \frac{(a^k - 1)}{(a - 1)}c \right) \mathrm{mod}\,m. \tag{72}$$

A linear congruential sequence will begin to repeat after producing at most $m$ distinct elements in the range $[0, m-1]$, and the maximum period $m$ is attained only for certain values of $m$, $a$ and $c$. With some care, the sequence can be constructed to have sufficient randomness for the purpose in hand, as measured by the distribution of the elements over the range $[0, m-1]$ and by the lack of significant correlation between successive elements. Real–number values on the intervals $[0, 1)$, $[-\pi, \pi)$, $[0, 2\pi)$, etc. may be obtained by an appropriate normalisation.

Knuth [12] presents a theorem, proved at some length using number theory, which states that a linear congruential sequence has maximum period of length $m$ if and only if

1. $c$ is relatively prime to $m$;

2. $b = a - 1$ is a multiple of $p$, for every prime $p$ dividing $m$;

3. $b$ is a multiple of 4, if $m$ is a multiple of 4.

If the conditions indicated by the theorem are met then a sequence of length $m$ will contain every integer between 0 and $m - 1$ inclusive exactly once. Due to the periodicity of the sequence the choice of the starting value $X_0$ within this range is essentially irrelevant.

The constraints on $m$, $a$ and $c$ imposed by the above theorem are rather weak and are satisfied by many possible sets of values. Indeed, there is no guarantee that a linear congruential sequence based on such a set of values will form the basis of a useful random number generator. There is some additional theory [12] to support the use of particular forms of $a$ and $c$, but in general the sequence resulting from each new set of parameters must be tested to ensure that its behaviour is satisfactory. A large number of theoretical and statistical tests is available to check many different aspects of the behaviour of the sequence; Knuth provides a comprehensive list.

## The Spectral Test

The spectral test is a theoretical test of the properties of the sequence resulting from a particular choice of the multiplier $a$ for a given modulus $m$. It does not consider the effect of the increment $c$. The theory behind the test makes use of the multidimensional discrete Fourier transform pair defined as

$$
\begin{aligned}
f(\underline{s}) &= \sum_{t_1=0}^{m-1} \ldots \sum_{t_n=0}^{m-1} F(\underline{t}) e^{2\pi i \underline{s}.\underline{t}/m} \\
F(\underline{t}) &= \frac{1}{m^n} \sum_{s_1=0}^{m-1} \ldots \sum_{s_n=0}^{m-1} f(\underline{s}) e^{-2\pi i \underline{s}.\underline{t}/m}
\end{aligned}
$$

where the vectors $\underline{s}$ and $\underline{t}$ of length $n$ have integer components $0 \le s_i, t_i < m$. The functions $F(\underline{t})$ and $f(\underline{s})$ are complex–valued in general and periodic in the sense that $F(\underline{t}) = F(\underline{t} \bmod m)$ and $f(\underline{s}) = f(\underline{s} \bmod m)$. For the purpose of the spectral analysis the function $F(\underline{t})$ is defined as

$$
F(\underline{t}) = \frac{1}{m^n} \sum_{k=0}^{m-1} \delta_{X_k t_1} \delta_{X_{k+1} t_2} \ldots \delta_{X_{k+n-1} t_n}
$$

where $\delta_{X_i t_j} = 1$ if $X_i = t_j$ and is zero otherwise. Thus $F(\underline{t})$ is the probability density of the occurrence of the ordered set of integers $(t_1, \ldots, t_n)$ as a sub-sequence of the random sequence $(X_0, \ldots, X_{m-1})$, taken over all possible such sub–sequences. For example, if $n = 1$ then $F(t_1) = 1/m$, since only the term in the summation for which $X_k = t_1$ survives. Similarly, for $n = 2$ only the term for which $X_k = t_1$ *and* $X_{k+1} = t_2$ survives and $F(t_1, t_2) = 1/m^2$. Clearly the general result is $F(\underline{t}) = 1/m^n$, and this will hold for any finite sequence $(X_0, \ldots, X_{m-1})$ that is truly random. The Fourier transform relations then give $f(\underline{s})$ as

$$
f(\underline{s}) = \frac{1}{m} \sum_{k=0}^{m-1} e^{2\pi i (X_k s_1 + X_{k+1} s_2 + \ldots + X_{k+n-1} s_n)/m}, \tag{73}
$$

and in order to recover the result $F(\underline{t}) = 1/m^n$ from the inverse transform then it must be the case that $f(\underline{s}) = 1$ if the vector $\underline{s} = 0$ and $f(\underline{s}) = 0$ otherwise.

For a linear congruential sequence the elements $X_{k+i}$ are defined for all $i$ by (72), and substituting (72) into (73) yields

$$
\begin{aligned}
f(\underline{s}) &= \frac{1}{m} \sum_{k=0}^{m-1} \exp\left[ \frac{2\pi i}{m} \left( s(a) X_k + \frac{s(a) - s(1)}{a-1} c \right) \right] \\
&= \frac{1}{m} \sum_{k=0}^{m-1} \exp\left[ \frac{2\pi i}{m} \left( s(a) k + \frac{s(a) - s(1)}{a-1} c \right) \right]
\end{aligned} \tag{74}
$$

where $s(a) = s_1 + s_2 a + s_3 a^2 + \ldots + s_n a^{n-1}$, and where the second step follows since the summation is over the full period $m$ and hence then all elements $X_k$ of the sequence are included. Thus

$$
\begin{aligned}
f(\underline{s}) &= \frac{1}{m} \exp\left[ \frac{2\pi i c}{m} \left( \frac{s(a) - s(1)}{a-1} \right) \right] \\
&\times \left[ 1 + \exp\left( \frac{2\pi i s(a)}{m} \right) + \ldots + \exp\left( \frac{2(m-1)\pi i s(a)}{m} \right) \right]
\end{aligned}
$$

and the series may be summed to give

$$
f(\underline{s}) = \exp\left[ \frac{2\pi i c}{m} \left( \frac{s(a) - s(1)}{a-1} \right) \right] \tag{75}
$$

if $s(a)$ is an integer multiple of $m$, and $f(\underline{s}) = 0$ otherwise.

Now, by the usual interpretation of the Fourier transform, the quantity $f(\underline{s})/m^n$ is the amplitude of the $n$-dimensional Fourier component with wavenumber vector $\underline{s}$ having magnitude

$$s^{(n)} = \sqrt{s_1^2 + s_2^2 + \ldots + s_n^2}. \tag{76}$$

Then (75) may be interpreted as the spectrum of the random sequence $X_0, \ldots, X_{m-1}$. If the sequence is truly random then the spectrum will be identically zero for all $\underline{s}$ except $\underline{s} = 0$, when it is equal to unity. If the sequence is not truly random it will suffer from sequential correlations and the spectrum will contain non–zero entries for $\underline{s} \neq 0$. Such entries can occur only when the components of the wavenumber vector $\underline{s}$ satisfy the relation

$$s(a) = s_1 + s_2 a + s_3 a^2 + \ldots + s_n a^{n-1} = 0 \bmod m \tag{77}$$

and in each case there is a corresponding wavenumber vector magnitude $s^{(n)}$. The minimum value $\nu_n$ of $s^{(n)} > 0$ for which $f(\underline{s})$ is non–zero provides an indication of the degree of randomness of the sequence - if $\nu_n$ is large then the sequence is likely to be a good approximation to a truly random sequence.

For the purpose of testing, this idea is made more precise by combining (77) and (76) to yield a single expression defining an ellipsoid in $n$-dimensional space:

$$(x_1 m - x_2 a - x_3 a^2 - \ldots - x_n a^{n-1})^2 + x_2^2 + \ldots + x_n^2 = s_n^2$$

The volume of the ellipsoid is given by

$$C_n = \frac{\pi^{n/2} s_n^n}{(n/2)! m}$$

where the factorial operator is applied as standard for even $n$, and is defined for odd $n$ as

$$\left(\frac{n}{2}\right)! = \left(\frac{n}{2}\right)\left(\frac{n}{2} - 1\right) \ldots \left(\frac{1}{2}\right)\sqrt{\pi}.$$

The volume $C_n$ is the figure of merit for the spectral test. For given values of $m$ and $a$ it is necessary to find the minimum wavenumber vector magnitude $\nu_n$ for all sets of integers $s_1, \ldots, s_n$ satisfying (77). Knuth provides an algorithm, notes that the value of $C_1 = 2$ always, and suggests that values of $C_n$ should be evaluated for $n = 2, 3, 4, 5$ and $6$. A sequence has passed the spectral test if $C_n > 0.1$, and has passed "with flying colours" if $C_n > 1.0$.

## Implementation and Testing of Linear Congruential Sequences

In order for the period of the sequence to be as long as possible it is necessary to choose the modulus $m$ to be as large as possible. In principle, with access to machine–level programming, $m$ can be made very large. Here, in order to ensure portability between different computers, the value of $m$ is constrained by the maximum integer value that can be represented using a standard high–level programming language. This implies that the computation of $X_{n+1}$ from $X_n$ must never produce an intermediate result that is larger than the maximum representable integer $r$, in order to avoid integer overflow errors. Thus $aX_n + c \leq r$, and since the maximum possible value of $X_n$ is $m-1$, the maximum value of $m$ is given by

$$m \leq 1 + \frac{r - c}{a}. \tag{78}$$

In practice, using standard four–byte signed integers, $r$ takes the value $2^{31} - 1 = 2147483647$. There is little theoretical guidance on choosing a value of the increment $c$, but Knuth suggests that it should be a prime number close to the value $(\frac{1}{2} - \frac{1}{6}\sqrt{3})m$. Then candidate values of $m$ and $a$ can be deduced using (78) and the theorem given above.

Six different sets of values for $m$, $a$ and $c$ for $r < 2^{31} - 1$ were taken from [13] and were checked for compliance with the conditions of the theorem, thus ensuring that the resulting linear congruential

sequence has the maximum period length $m$. A seventh set of values for $m$, $a$ and $c$ was also produced subject to the same set of constraints but having a longer period. The period length for all seven sequences was checked directly by evaluating the entire sequence numerically. Equidistribution of the elements of the sequence is guaranteed over the full period length, but was checked for shorter lengths using the Kolmogorov–Smirnov (KS) test [12, 13]. Subsequences of length 1000, 10000 and 100000 were generated using interval $[0, 1)$. In each case the probability that the elements of the subsequence belong to a distribution having a uniform probability density function (linearly increasing cumulative distribution function) was evaluated from the KS statistic, and the results are shown in Table 1.

| no. | $m$ | $a$ | $c$ | test | 1000 | 10000 | 100000 |
|-----|-----|-----|-----|------|------|-------|--------|
| 1. | 259200 | 7141 | 54773 | 1 | 0.5138 | 0.9936 | 1.0000 |
|    |        |      |       | 2 | 0.8076 | 0.8140 | 1.0000 |
|    |        |      |       | 3 | 0.3440 | 0.9566 | 0.9962 |
|    |        |      |       | 4 | 0.1478 | 0.9932 | 1.0000 |
|    |        |      |       | 5 | 0.4211 | 0.9982 | 0.9935 |
| 2. | 134456 | 8121 | 28411 | 1 | 0.1430 | 0.1086 | 0.9977 |
|    |        |      |       | 2 | 0.1032 | 0.5458 | 0.9778 |
|    |        |      |       | 3 | 0.3605 | 0.1325 | 0.9936 |
|    |        |      |       | 4 | 0.8623 | 0.1591 | 0.7141 |
|    |        |      |       | 5 | 0.7970 | 0.5412 | 0.8303 |
| 3. | 243000 | 4561 | 51349 | 1 | 0.4896 | 0.7039 | 0.9994 |
|    |        |      |       | 2 | 0.4191 | 0.8469 | 0.9011 |
|    |        |      |       | 3 | 0.4565 | 0.8724 | 0.9378 |
|    |        |      |       | 4 | 0.9980 | 0.5992 | 0.8482 |
|    |        |      |       | 5 | 0.0315 | 0.4078 | 0.9970 |
| 4. | 714025 | 1366 | 150889 | 1 | 0.9701 | 0.5001 | 0.9996 |
|    |        |      |       | 2 | 0.8738 | 0.4586 | 0.9998 |
|    |        |      |       | 3 | 0.3552 | 0.6645 | 0.9540 |
|    |        |      |       | 4 | 0.4474 | 0.5972 | 0.9815 |
|    |        |      |       | 5 | 0.9768 | 0.1184 | 0.9568 |
| 5. | 214326 | 3613 | 45289 | 1 | 0.8119 | 0.6180 | 1.0000 |
|    |        |      |       | 2 | 0.4294 | 0.6703 | 1.0000 |
|    |        |      |       | 3 | 0.2010 | 0.8063 | 1.0000 |
|    |        |      |       | 4 | 0.8584 | 0.9269 | 1.0000 |
|    |        |      |       | 5 | 0.6399 | 0.7103 | 1.0000 |
| 6. | 139968 | 3877 | 29573 | 1 | 0.4101 | 0.5215 | 0.5806 |
|    |        |      |       | 2 | 0.7501 | 0.3271 | 0.4429 |
|    |        |      |       | 3 | 0.5296 | 0.6256 | 0.9585 |
|    |        |      |       | 4 | 0.9758 | 0.9437 | 0.7908 |
|    |        |      |       | 5 | 0.7854 | 0.3934 | 0.8586 |
| 7. | 1000000 | 2141 | 211319 | 1 | 0.6394 | 0.9276 | 0.9956 |
|    |        |      |       | 2 | 0.6731 | 0.9028 | 0.9924 |
|    |        |      |       | 3 | 0.1584 | 0.3697 | 0.9793 |
|    |        |      |       | 4 | 0.3685 | 0.8823 | 0.9294 |
|    |        |      |       | 5 | 0.2835 | 0.5841 | 0.9318 |

Table 1: Parameters and Kolmogorov–Smirnov test results for linear congruential sequences

The results reveal considerable variability between different sequences, and between the subsequences of each sequence. In general the subsequences of length 1000 have rather poor equidistribution properties, and in almost all cases there is a significant improvement for subsequences of length 10000. As expected, subsequences of length 100000 show the highest probabilities of equidistribution. These findings were

checked using the $\chi^2$ test and the results were found to be in good qualitative agreement.

Finally the spectral test was applied to each sequence and the results are shown in Table 2. Clearly all

| no. | $C_2$ | $C_3$ | $C_4$ | $C_5$ | $C_6$ |
|---|---|---|---|---|---|
| 1. | 2.003 | 2.787 | 0.5121 | 0.2608 | 0.4377 |
| 2. | 1.927 | 0.7260 | 0.5597 | 0.5218 | 4.615 |
| 3. | 2.626 | 0.4701 | 0.5596 | 0.2192 | 0.1240 |
| 4. | 1.883 | 2.534 | 3.950 | 0.1580 | 0.1589 |
| 5. | 0.7355 | 1.570 | 1.304 | 0.3154 | 1.786 |
| 6. | 3.080 | 2.312 | 1.220 | 1.331 | 2.026 |
| 7. | 0.7587 | 2.042 | 0.6610 | 2.551 | 2.646 |

Table 2: Parameters and spectral test results for linear congruential sequences

of the sequences pass the spectral test (ie $C_n > 0.1$) by some margin and therefore are well suited for use as random number generators. In particular, the new sequence (no.7) has the longest period (1000000) and has $C_n$ values at least as high as those of any of the other sequences. This sequence lies close to the practical limit on the period as set essentially by the value of $r$.

## Practical Random Number Generators

The period length of all of the above sequences remains much too short for use in generating initial turbulent fields for DNS and LES. In order both to lengthen the period and to increase the the number of distinct values in the sequence it is necessary to combine the output from at least two different sequences. Taking an element $X_1$ from a linear congruential sequence of length $m_1$ and an element $X_2$ from a second linear congruential sequence of length $m_2$ a new combined integer value $X_c$ may be formed as

$$X_c = X_1 m_2 + X_2$$

where now $X_c$ is an element of a sequence of integers that takes all values between 0 and $m_1 m_2 - 1$ inclusive. It should be noted that the combined sequence is capable of producing integer values that are much larger than the maximum representable integer $r$, and hence it is necessary to use real arithmetic to evaluate $X_c$.

The combined sequence is not a linear congruential sequence, and it is likely to be contaminated by any sequential correlations that are present in the constituent sequences. At best the correlation length of the combined sequence will be set by the modulus $m_2$ and the advantage of the greatly increased period will be much reduced. In order to break up unwanted correlations Knuth recommends a shuffling procedure using a table of about 100 entries, and chooses 97 as a suitably close prime number. Initially the table is filled with elements from the combined sequence, and is then accessed using the elements of a third linear congruential sequence to generate a pseudo–random index to the table. Each table entry that is selected is taken to be the required random number to be output, and is then replaced with a new element obtained from the combined sequence. This procedure is intended to allow the full period of the combined sequence to be used without significant correlation.

Two different random number generators based on combined sequences with shuffling were constructed from the linear congruential sequences listed in Table 1. The first is presented in [13] and uses sequence no.1 for the low–order segment, sequence no.2 for the high–order segment, and sequence no.3 to index the shuffling table. The second is new and uses sequence nos.4, 5 and 6 respectively for the same purposes. Even without shuffling the period of each of these combined sequences is very large ($m_1 m_2 = 34,850,995,200, m_4 m_5 = 153,034,122,150$), and with shuffling the period becomes effectively infinite.

The equidistribution properties of each combined and shuffled random number generator were tested using the KS test and checked using the $\chi^2$ test. Results from the KS test are shown in Table 3. Both generators show a high probability of equidistribution for subsequences of length 100000, but the first

| no. | | $m$ | $a$ | $c$ | test | 1000 | 10000 | 100000 |
|-----|-----------|--------|------|--------|------|--------|--------|--------|
| 1. | low–order | 259200 | 7141 | 54773 | 1 | 0.1172 | 0.7478 | 0.9940 |
| | high–order | 134456 | 8121 | 28411 | 2 | 0.2422 | 0.9799 | 1.0000 |
| | shuffle | 243000 | 4561 | 51349 | 3 | 0.3977 | 0.9982 | 1.0000 |
| | | | | | 4 | 0.1363 | 0.9863 | 0.9999 |
| | | | | | 5 | 0.3706 | 0.9999 | 0.9998 |
| 2. | low–order | 714025 | 1366 | 150889 | 1 | 0.4026 | 0.5610 | 0.9086 |
| | high–order | 214326 | 3613 | 45289 | 2 | 0.2395 | 0.1447 | 0.9636 |
| | shuffle | 139968 | 3877 | 29573 | 3 | 0.3016 | 0.1657 | 0.9913 |
| | | | | | 4 | 0.4612 | 0.7479 | 0.9990 |
| | | | | | 5 | 0.4751 | 0.9547 | 0.9754 |

Table 3: Parameters and Kolmogorov–Smirnov test results for combined sequences with shuffling

generator has markedly better equidistribution properties for subsequences of length 10000, while the second generator has a slight advantage for short subsequences.

## Correlation Functions

Perhaps the most sensitive test of sequential correlation is to evaluate the discrete correlation function

$$c_i = \sum_n X_{n+i}^{(1)} X_n^{(2)}$$

for two subsequences $X_n^{(1)}$ and $X_n^{(2)}$. This is most efficiently done using the FFT algorithm and the discrete correlation theorem

$$\hat{c}_k = \hat{X}_k^{(1)} \left( \hat{X}_k^{(2)} \right)^*$$

where the hat denotes a Fourier transform and the $*$ a complex conjugate. It is also convenient to use the normalisation

$$Y_n = 2 \left( \frac{X_n}{m} \right) - 1$$

such that the normalised random variable $Y_n$ is defined on the interval $[-1, 1)$ and has zero mean. If the subsequences $Y_n^{(1)}$ and $Y_n^{(2)}$ are uncorrelated then the discrete correlation function

$$c_i^{Y(1,2)} = \sum_n Y_{n+i}^{(1)} Y_n^{(2)}$$

will be identically zero for all values of the lag $i$. The normalised discrete autocorrelation function $(Y_n^{(1)} = Y_n^{(2)} = Y_n)$

$$\bar{c}_i^Y = \frac{\sum_n Y_{n+i} Y_n}{\sum_n Y_n^2}$$

is of particular interest: for truly random $Y_n$ it takes the value unity for $i = 0$ and is zero for all other values of $i$.

The function $\bar{c}_i^Y$ was evaluated for all of the linear congruential sequences listed in Table 1, using the full period of the sequence in each case. Results are shown in Figure 7. Clearly none of the sequences is free from some degree of correlation, as revealed by the occurrence of isolated sharp spikes in the autocorrelation function. For sequences having even period length $m$ there is a spike of magnitude $-1/2$ at a lag of $m/2$ - it can be shown [12] using the expression (72) that this is an intrinsic property of the linear congruential method. The cross–correlation function $c_i^{Y(1,2)}$ was evaluated for each linear congruential sequence by changing the starting value $Y_1^{(2)}$ - as expected this simply shifts the pattern

22

(a) Sequence no.1

(b) Sequence no.2

(c) Sequence no.3

(d) Sequence no.4

(e) Sequence no.5
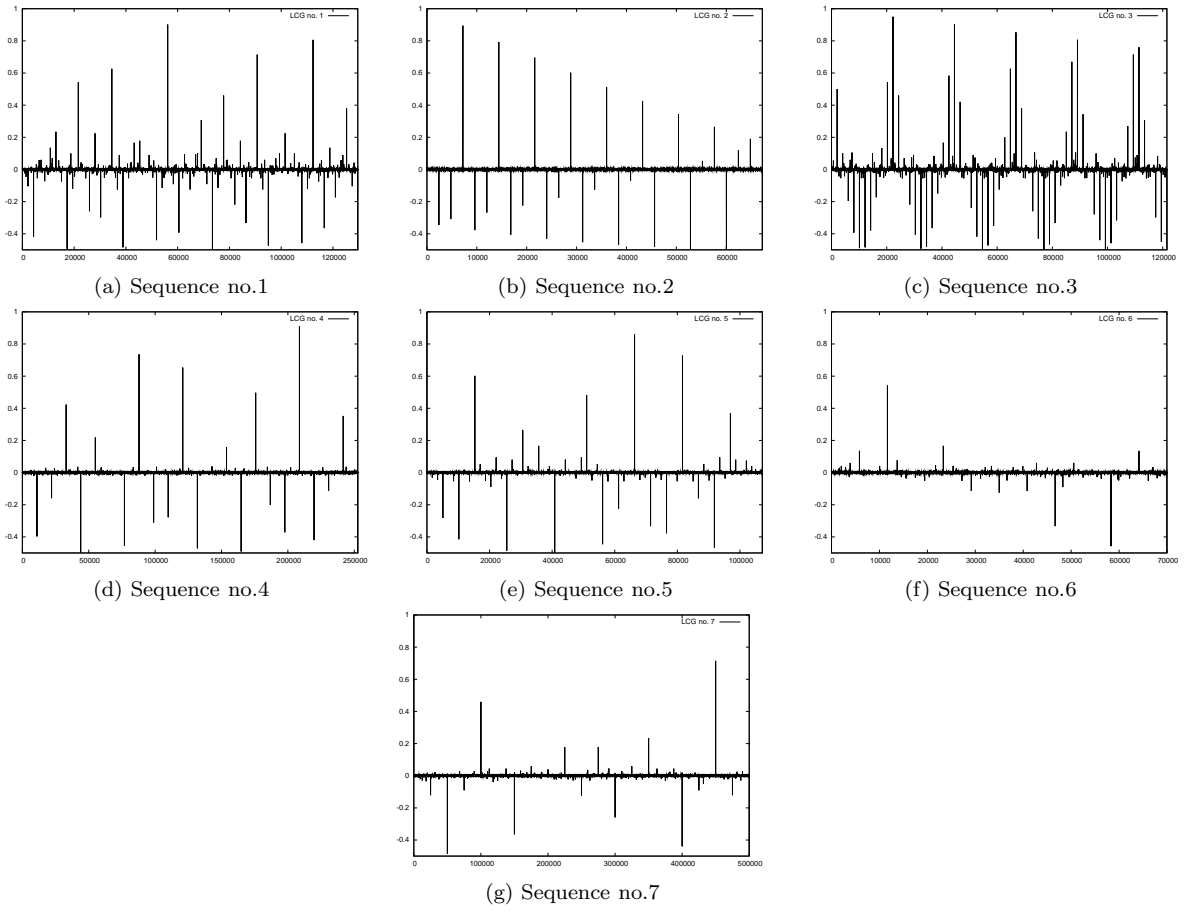
(f) Sequence no.6

(g) Sequence no.7

Figure 1: Autocorrelation functions for linear congruential sequences

observed in the autocorrelation function, by an amount that depends on the location of the starting value within the sequence.

Autocorrelation functions were also evaluated for the combined and shuffled sequences, and results are shown in Figure 2. Here it is not feasible to use the full period of the sequence and a sample of



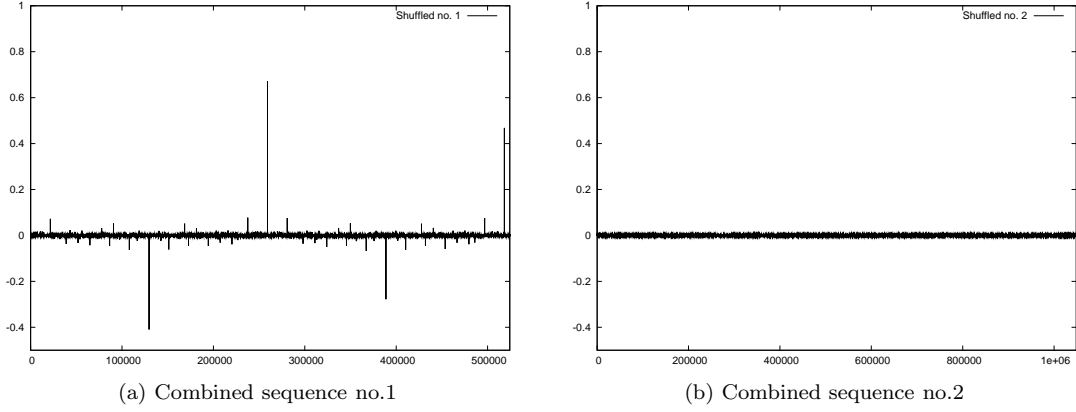(a) Combined sequence no.1            (b) Combined sequence no.2

Figure 2: Autocorrelation functions for the combined and shuffled sequences

length 1048576 was used for sequence no.1, and 2097152 for sequence no.2. For sequence no.1 there is evidence of non–zero correlation at the period length of the linear congruential sequence used to generate the low–order segment, but the magnitude of the correlation spikes has been reduced by the shuffling algorithm. Sequence no.2 appears to be essentially free of significant correlation, even over the much longer sample size tested. Tests on the length of the shuffling array with values up to 997 revealed very little sensitivity to this parameter. Cross–correlation of the combined and shuffled sequence with different starting values showed very low values throughout.

Finally the combined and shuffled sequences were sub–sampled by taking every third element, starting in turn with elements 1, 2 and 3. This reflects the manner in which the sequence is likely to be used for initialisation of a DNS. Autocorrelation of each sub–sampled sequence showed similar behaviour to that of the full sequence, while cross–correlation again returned very low values.

## Conclusions

Investigation of the properties of random number generators suitable for use in DNS of turbulent flow has been carried out using theoretical, statistical and correlation techniques. An overriding requirement is that the random number generator routine should be portable, and therefore must be written in a standard high level language. This places a restriction on the maximum integer value that can be represented. Linear congruential sequences are computationally efficient and may be designed to have well–defined properties, but testing remains essential. Such sequences are periodic on lengths which are too short for present purposes, and also exhibit regular correlations on fractions of the period length. Two linear congruential sequences may be combined to yield a sequence having very much greater period length, and a simple shuffling algorithm may be used to smear out unwanted correlations and further to extend the period length to values well beyond those of present concern. Such combined and shuffled random number generators have adequate equidistribution properties across the interval of interest, and are reasonably free of correlations that could contaminate an initial turbulent field. In particular, there is no appreciable correlation between subsequences consisting of every third element of the main sequence: this ensures that the angles required at each point are uncorrelated. Similarly, there is no appreciable correlation between sequences generated using different starting values: this ensures that initial turbulent fields generated by separate processors of a parallel computer will remain uncorrelated provided that a different seed is used to initialise the random number generator on each processor.

# References

[1] S.A. Orszag: Numerical methods for the simulation of turbulence, Phys. Fluids Suppl. II, 250–257, 1972.

[2] R.S. Rogallo: Numerical experiments in homogeneous turbulence, NASA Tech. Memo. 81315, 1981.

[3] M.J. Lee, W.C. Reynolds: Numerical experiments on the structure of homogeneous turbulence, Technical Report TF–24, Thermosciences Division, Dept. of Mechanical Engineering, Stanford University, 1985.

[4] G.K. Batchelor: *The Theory of Homogeneous Turbulence*, Cambridge University Press, 1953.

[5] U. Schumann, G.S. Patterson: Numerical study of pressure and velocity fluctuations in nearly isotropic turbulence, J. Fluid Mech. **88**, 4, 685–709, 1978.

[6] G.K. Batchelor, A.A. Townsend: Decay of turbulence in the final period, Proc. Roy. Soc. Lond. **A194**, 527–543, 1948.

[7] A.S. Monin and A.M. Yaglom: *Statistical Fluid Mechanics*, Vol.1, Mechanics of Turbulence, ed. J.L. Lumley, MIT Press, 1971.

[8] C. Temperton: A generalised prime factor FFT algorithm for any $N = 2^p 3^q 5^r$, SIAM J. Sci. Stat. Comp. **13**, 676–686, 1992.

[9] R.J. Allan: Parallel application software on high performance computers: serial and parallel FFT routines, CSED Report, Daresbury Laboratory, UK, ISSN 1362–0193, 2nd ed., 1999.

[10] J.O. Hinze: *Turbulence*, McGraw–Hill, 2nd ed., 1975.

[11] J.A. Eisele, R.M. Mason: *Applied Matrix and Tensor Analysis*, John Wiley and Sons, 1970.

[12] D.E. Knuth: *The Art of Computer Programming*, Vol.2, Seminumerical Algorithms, Addison–Wesley, 1969.

[13] W.H. Press, S.A. Teukolsky, W.T. Vetterling, B.P. Flannery: *Numerical Recipes*, Cambridge University Press, 3rd ed., 2007.